




Hydrogen concentration dependence of phase transformation and microstructure modification in metastable titanium alloy β -21S

Jing Wen^{1,2,*} , Eric Fleury¹, Fei Cao³, and Nathalie Allain¹

¹LEM3, UMR CNRS 7239, Arts et Métiers ParisTech, Université de Lorraine, 57000 Metz, France

²CNRS, Institut Néel, Université Grenoble Alpes, 38000 Grenoble, France

³Department of Metallurgical Engineering, University of Utah, Salt Lake City, UT, USA

Received: 14 March 2020

Accepted: 13 November 2020

Published online:
30 November 2020

© Springer Science+Business
Media, LLC, part of Springer
Nature 2020

ABSTRACT

The present study aims at revealing the relationships between hydrogen concentration and phase structure, as well as microstructure modification in the β -metastable β -21S titanium alloy. The β -bcc phase can accommodate a large number of interstitial atoms, and hydrogenation by means of molecular hydrogen gas was employed in the present work. The phase structure as well as the microstructure of this alloy was found to be strongly dependent on hydrogen concentration. At lower hydrogen concentration ($H/M \leq 0.300$), the microstructure consisting of the single β -phase revealed that the interstitially dissolved hydrogen atoms expanded the bcc lattice and inhibited the decomposition of the β phase upon cooling. The introduction of hydrogen beyond $H/M = 0.300$ was found to generate a large amount of internal stresses in the microstructure inducing the formation of metastable phases α'' in the form of lamellae and ω in the form of nanoparticles. The generation of the nanosized ω -phase was presumed to relax the strain caused by the volume expansion (2.28%) from the hydrogen-containing β phase to the α'' martensite.

Introduction

The metastable β -titanium alloy β -21S (Ti-15Mo-3Nb-3Al-0.2Si) commonly obtained upon high cooling rate has become a promising candidate for structural applications as structure components in hydrogen-fueled hypersonic planes owing to its high specific

strength and good formability as well as its excellent elevated temperature performance [1, 2]. The crystallographic structure of the phase in the β -21S alloy is dependent on the final thermal treatment. In solution-annealed state, though the BCC β phase is the dominant phase, a very low volume fraction of HCP athermal ω phase has been detected by

Handling Editor: David Balloy.

Address correspondence to E-mail: jing.wen@neel.cnrs.fr

<https://doi.org/10.1007/s10853-020-05568-5>

numerous investigations [3–7]. In aged condition, the ω phase transforms into the HCP α phase and the β -21S alloy exhibits a two-phase ($\alpha + \beta$) microstructure with the volume fraction of both phases depending upon the aging condition [3]. Another phase detected in metastable β -Ti alloys, e.g., Ti-10 V-2Fe-3Al [8], upon quenching or mechanical deformation is the martensite α'' phase (orthorhombic structure). However, as far as we know, this martensite α'' phase has not been reported for the β -21S alloy.

Hydrogen is present in β -21S alloy, in many cases inadvertently, as a collateral result of processing, corrosion, etc. Since the β -21S alloy exhibits a large solubility of hydrogen in the bcc phase and does not readily form hydrides, this alloy has been assessed to be rather resistant to hydrogen, except probably under relatively high hydrogen pressures [1]. Besides, hydrogen can be used as a temporary alloying element to facilitate the thermomechanical processing of titanium products by reducing the flow stress [9–11]. Numerous studies have been carried out to understand how hydrogen influences the mechanical behavior of β -21S alloy [12–18]. However, these studies often provide contradictory results ascribed to the means of introducing hydrogen, hydrogen interaction with defects and the strain rate of the mechanical testing investigations.

A detailed study of hydrogen effect on the deformation behavior of β -21S alloy undertaken by Teter and co-workers [7] demonstrated that the hydrogen-induced ductile–brittle transition took place abruptly at a critical hydrogen concentration that decreased with temperature. The mechanism behind the sharp loss of ductility is supposed to be the hydrogen-induced decohesion [19–21]. Despite these thorough studies of the hydrogen effect on deformation behavior, a detailed investigation of microstructure modification with respect to different hydrogen concentrations in β -21S alloy was not reported [7]. In addition to being a β -phase stabilizer in β -21S alloy, hydrogen is expected to affect the sequence of phase transformation upon cooling as it has been reported in $\alpha + \beta$ Ti-6Al-4 V [22]. Upon hydrogenation, the hydrogen atoms can preferentially be trapped by the structural defects such as vacancies, dislocations, grain/phase boundaries, etc., which causes the distortion of the crystal lattice to some extent [23]. Since microstructure is the governing factor that determines the performance of titanium products, the objective of the present work is to

follow the microstructure modification with respect to hydrogen concentration and to quantify the relationship between phase structure and hydrogen concentration.

Materials and methods

The material used was the TIMETAL®21S titanium alloy in the form of a plate (thickness of 1.8 mm) obtained by solution annealing. To ensure a homogeneous distribution of hydrogen through the sample volume, hydrogen was introduced by gas method [24, 25] in the present work. The hydrogen charging procedure was similar to that employed in Ref. [7]. Firstly, the samples were positioned in a furnace at 10^{-4} Pa; then the furnace temperature was increased up to 1123 K (a single β -phase field), and subsequently the H_2 gas with argon at a predetermined pressure was introduced into the furnace which was maintained for a sufficient time (30–60 min) to achieve equilibrium throughout the specimen volume, i.e., homogenous dispersion of hydrogen. Different hydrogen concentrations were obtained by controlling the partial pressure of hydrogen gas (Ar/ H_2 ratio) and the charging time. The amount of hydrogen dissolved in the sample was measured via the inert gas fusion instrument (LECO TCH-600). The hydrogen gas pressures and the corresponding hydrogen concentrations are presented in Table 1.

Since hydrogen lowers the β -transus temperature for the β -titanium alloy [23], it promotes the stability of the β -phase upon cooling. Following this consensus, the hydrogen-induced microstructure modification was inspected using a combined analysis of the X-ray diffraction (XRD), scanning electron microscopy (SEM)-based electron backscatter diffraction (EBSD) and transmission electron microscopy (TEM) characterizations. The XRD experiments were performed using a D8 Endeavor (from Bruker) with a Cu-K α at a step of 0.01 $^\circ$ /s. For EBSD characterization, the samples were electropolished at 2 $^\circ$ C for 5 s in an electrolyte of 10% perchloric acid and 90% methanol. Then, the microstructure developed upon hydrogenation was investigated using a field-emission scanning electron microscope (JEOL-6500F) equipped with an EBSD detector and the AZtec acquisition software package (Oxford Instruments). To ensure an accurate determination of the orientation, the manual EBSD detecting mode was used to

Table 1 Ar/H₂ ratio, lattice parameter, hydrogen concentration and the full width at half maximum (FWHM) of (200)_β peak at each hydrogen concentration (H/M) for the studied β-21S alloys

Sample series	Ar/H ₂ ratio	Lattice parameter, Å	Hydrogen concentration		The full width at half maximum (FWHM) of (200) _β peak,
			(at %)	(H/M)	
AR	N/A	3.247	0.500	0.005	0.135 ± 0.003
HC-1	9	3.256	4.940	0.052	0.135 ± 0.003
HC-2	4	3.259	9.091	0.100	0.135 ± 0.003
HC-3	2.3	3.273	13.793	0.160	0.135 ± 0.003
HC-4	1.85	3.285	17.695	0.215	0.135 ± 0.003
HC-5	1.5	3.294	23.077	0.300	0.136 ± 0.003
HC-6	1	3.311	27.660	0.383	0.175 ± 0.005
HC-7	0.33	3.317	31.530	0.460	0.332 ± 0.008

determine the crystallographic orientation (in terms of Euler angles) of the observed microstructural constituents. By manually positioning the SEM beam to the lamellar regions, the orientation expressed in Euler angles (φ_1 , Φ , φ_2) corresponding to the measurement point was calculated by the software Aztec and recorded for each variant. The Euler angles represent a set of three characteristic rotations [26, 27] from the sample coordinate system to the crystal coordinate system. With the Euler angles, the coordinate transformation matrix can be established between the two coordinate systems. With the coordinate transformation matrices of the two phases, we can express the OR directions and the normal directions of the OR planes to the sample coordinate system (X-Y-Z) and project these directions to the XOY plane by stereographic projection [28, 29]. The coincident poles of the common directions and the common planes normal allow to determine the OR between the two phases. The crystallographic orientation relationships (OR) between the original β-phase and the newly formed phase represented with the stereographic projections of the corresponding OR plane normal and the OR direction of the phases were resolved using the rotational coordinate transformation matrices written in a MATLAB software [30].

For TEM observations, thin foils were extracted from as-received as well as hydrogenated β-21S alloys by ionic micromachining from the selected areas previously localized by SEM–EBSD. Extraction of thin foil was performed using a Focused Ion Beam (FIB) Zeiss Auriga 40 equipped with both electronic

and ionic columns (Gemini and Orsay Physics Cobra, respectively). To avoid the formation of the amorphous layer under the high-energy ion beam, the ionic micromachining was finished under a beam of 2 kV before extraction of the thin foil. Then, microstructures were examined in a Philips TEM200 CM at a working voltage of 200 kV for both imaging and phase identification.

Results and discussion

Hydrogen-induced phase transformation analyzed by XRD

Figure 1 shows microstructure aspect of the as-received β-21S alloy characterized by SEM and EBSD. The SEM-BSE image (Fig. 1a), the image quality map (Fig. 1b) and the inverse pole figure (IPF) map (Fig. 1c) reveal that the as-received sample is composed of equiaxed β grains with a mean grain size of about $35.0 \pm 2.0 \mu\text{m}$. No internal structure is observed in the interior of β grain, and no preferential grain orientation is noticed. Nevertheless, the {110} pole figure measured by XRD in Fig. 1d shows that a rather weak bcc-rolled texture is retained in the solution-annealed sample.

The XRD profiles for different hydrogen concentrations are shown in Fig. 2a. In the hydrogen concentration range $0 < H/M < 0.38$, the XRD patterns consist of the single β-phase; neither α-phase nor hydride precipitation is observed. However, the diffraction peaks gradually shifted toward lower 2θ

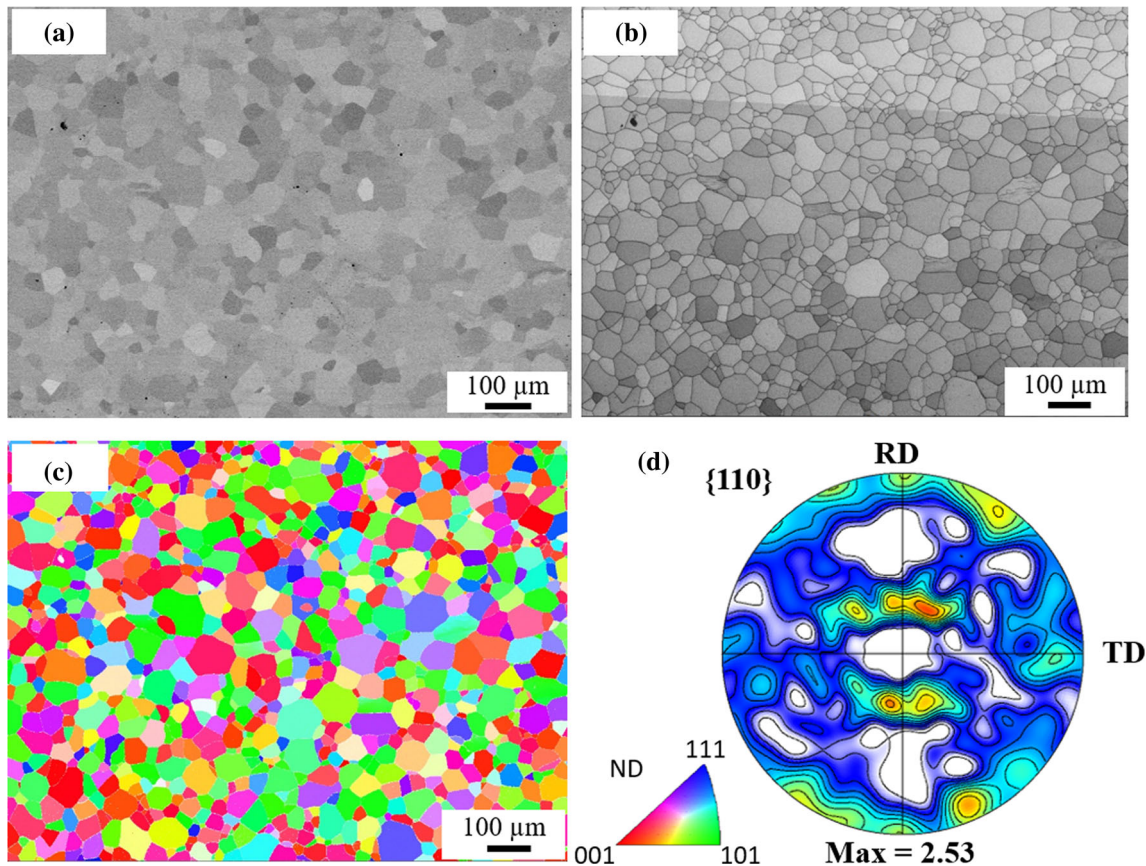


Figure 1 Microstructure of the as-received β -21S alloy, **a** SEM-BSE image; **b** and **c** EBSD image quality (IQ) and IPF maps of the same area; **d** $\{110\}$ pole figure measured by XRD.

angles with the hydrogen concentration increased to $H/M = 0.300$, which is due to lattice expansion of the β -phase caused by the interstitially dissolved hydrogen atoms. Moreover, it is worth noting that the x-ray diffraction peaks became broadened at hydrogen concentration exceeding 0.3 ($H/M > 0.3$). The broadening of the $(110)\beta$ peak in the XRD pattern for $H/M = 0.460$ was specially analyzed using a smaller scanning step $0.01^\circ/\text{s}$. Figure 2b reveals, in addition to the (110) peak corresponding to the β phase, the presence of the (002) and (111) peaks of the orthorhombic α'' phase, evidencing the formation of the α'' martensite. Its lattice parameters were thus determined to be $a = 0.3164$, $b = 0.4982$ and $c = 0.4658$ nm. Such a formation of the martensite α'' phase upon hydrogen charging has been reported by Qazi et al. in Ti-6Al-4V [22]. Indeed, at a high hydrogen concentration, the dissolved hydrogen atoms induce anisotropic deformation of the BCC lattice owing to segregation of hydrogen atoms at lattice defects [23]. The spacing between some planes is increased and decreased between some others. The

formation of the α'' martensite is supposed to result from anisotropic lattice deformation at high hydrogen concentration.

Since the XRD peaks became broadening at hydrogen concentration exceeding 0.3 ($H/M > 0.3$), the full width at half maximum (FWHM) value associated with the lattice strain [31] at each hydrogen concentration is given in Table 1. The extent broadening of $(200)\beta$ peak is negligible in the hydrogen concentration range $0.052 \leq H/M \leq 0.300$. Nevertheless, a significant increase in FWHM value is observed when the hydrogen concentration is higher than $H/M = 0.300$. The high FWHM value implies that a considerable amount of lattice strain is generated in the sample containing high hydrogen concentration.

By refining the obtained XRD patterns using the MAUD software [32], the lattice parameters at different hydrogen concentrations were determined. The relative change in the lattice parameter (i.e., $(a_H - a_0)/a_0$) as a function of hydrogen concentration is presented in Fig. 3, and the plot from the

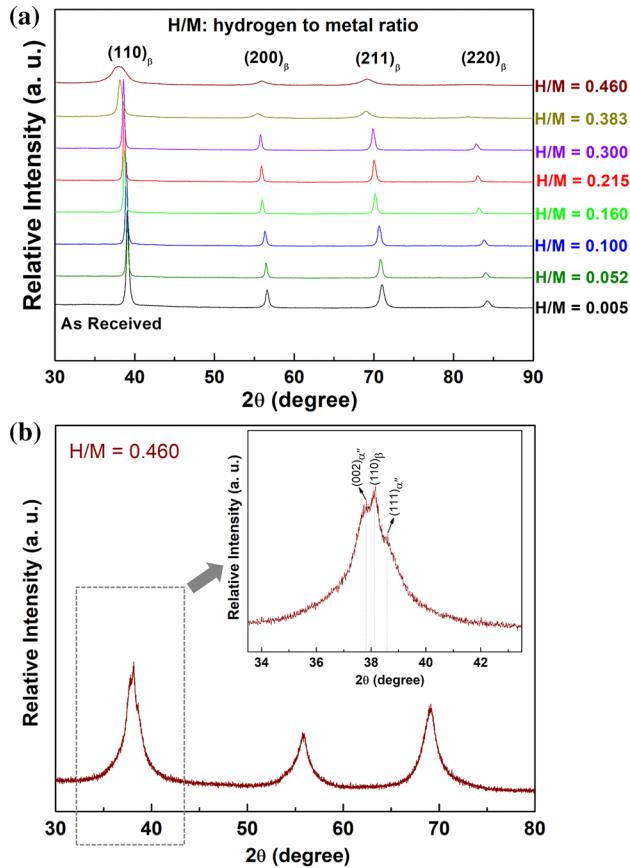


Figure 2 **a** XRD profiles of β -21S alloy containing different hydrogen concentrations and **b** XRD pattern measured at a smaller step $0.01^\circ/s$ for $H/M = 0.460$ (the insert plot is the enlargement of the selected zone, the (002) and (111) diffraction peaks corresponding to the martensite α'' phase is pointed by arrows).

reference data [7] is presented for comparison. In the hydrogen concentration range $0.052 \leq H/M \leq 0.460$, the lattice parameter of the β -phase varied approximately linearly with respect to the increasing hydrogen concentration, implying that no hydrides precipitation occurred in this concentration range and that the hydrogen atoms remained in β -solid solution. In comparison, the critical hydrogen concentration for hydride precipitation was estimated about $H/M = 0.67$ in [33] and the latter value is much higher than the one obtained in the present work. Performing a linear fit to the obtained data, the relative change in the lattice parameter as a function of hydrogen concentration was expressed as

$$[(a_H - a_O)/a_O] = 0.0508(H/M)$$

With a coefficient of correlation, $R = 0.996$. The equation showed a slightly larger value of the slope,

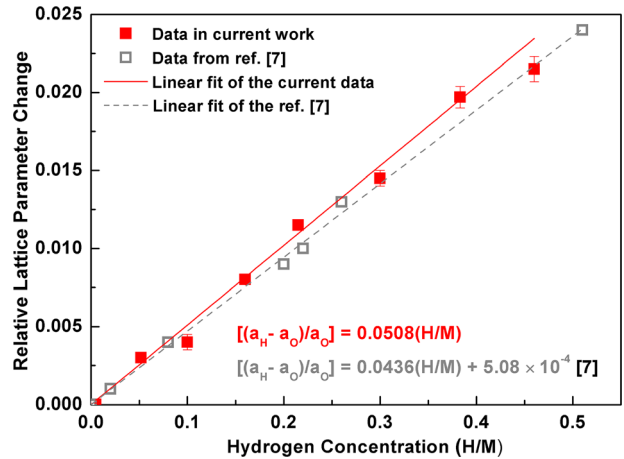


Figure 3 Relative change in the lattice parameter $[(a_H - a_O)/a_O]$ of the β -phase as a function of hydrogen concentration. Linear fitted data give $y = [(a_H - a_O)/a_O] = 0.0508(H/M)$ with a coefficient of correlation $R = 0.996$.

as compared to the one reported in the reference for the same alloy $[(a_H - a_O)/a_O] = 5.08 \times 10^{-4} + 0.0436(H/M)$ [7]. This minor difference could result from the measurement accuracy for hydrogen concentration.

Hydrogen-induced microstructure modification investigated by SEM–EBSD

Figure 4 shows the microstructure aspect of the hydrogenated β -21S alloy with different hydrogen concentrations. The SEM secondary electron image (SEI) of the hydrogenated β -21S alloy at hydrogen concentration $H/M = 0.215$ is presented in Fig. 4a, at which the abrupt ductile–brittle transition took place [7]. The microstructure consisted of only equiaxed β grains at $H/M = 0.215$, thus confirming the XRD analyses and that neither α -phase nor hydride was observed. However, with the hydrogen concentration increasing to $H/M = 0.380$, the original β grains were decorated with lamellar shaped constituents (Fig. 4b). As the hydrogen concentration was further increased to $H/M = 0.460$, numerous nets formed by the differently oriented lamellar microstructures appeared within the initial β -grains (Fig. 4c). Figure 5 presents the example Kikuchi patterns which are manually acquired from the lamellar constituents, the one being from the β -phase (Fig. 5a) and the other from the α'' phase (Fig. 5b). The calculated patterns using the lattice constants of the β -phase (in blue) and the α'' phase (in red) are superimposed with the

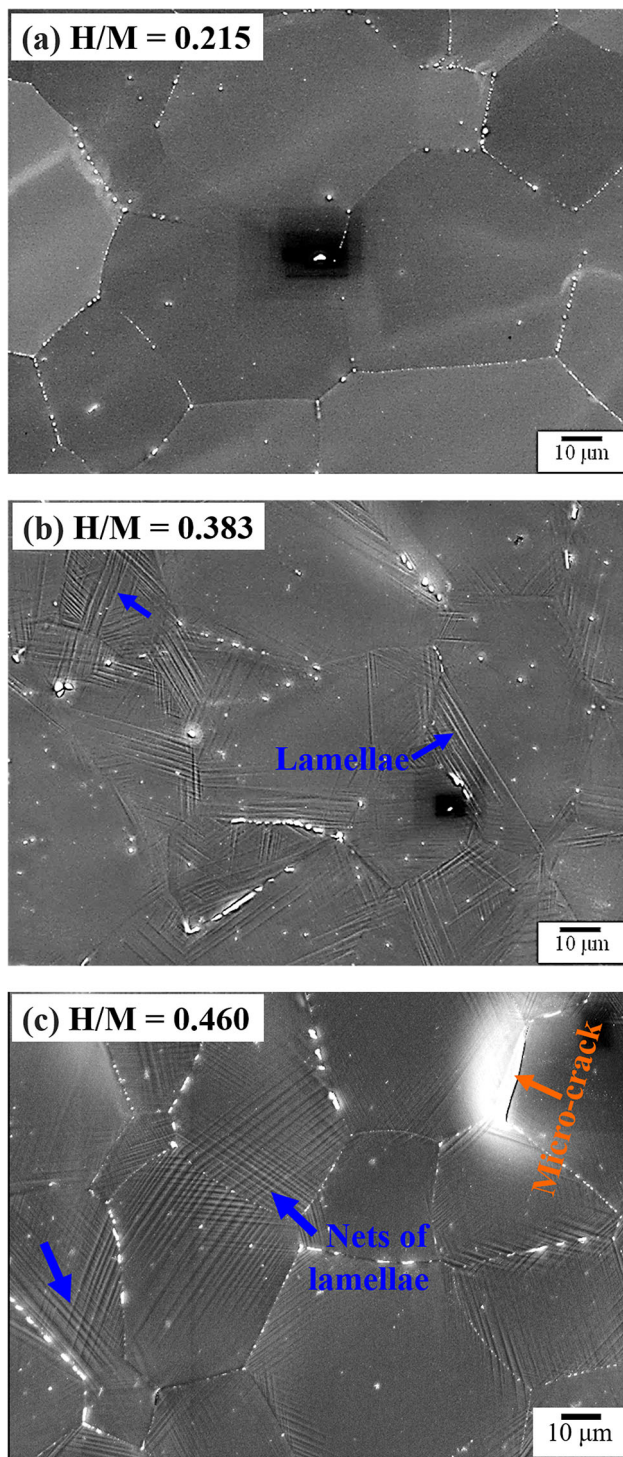


Figure 4 SEM-SEI micrographs taken from the cross section of the hydrogenated β -21S specimens, **a** $H/M = 0.215$, **b** $H/M = 0.380$ and **c** $H/M = 0.460$.

experimental ones. The lattice parameters ($a = 0.3164$, $b = 0.4982$ and $c = 0.4658$ nm) in Refs. [34, 35] were used to simulate the Kikuchi patterns (in blue) for the

orthorhombic α'' phase. The excellent fit between the experimental patterns and the calculated patterns further evidenced the formation of the α'' phase in the form of lamellae in the β -21S alloy upon hydrogen charging. The lamellae found in the present work exhibited the similar morphologies to those of the α'' martensite commonly formed in the quenched or mechanical deformed metastable β -titanium alloys [34–39].

To further examine the orientation relationship (OR) between the lamellae and the β phase, EBSD measurements were performed in the Grain A, as displayed in Fig. 6a. In this grain, several differently oriented lamellae (indicated by 1, 2, 3 and 4) within one β grain were revealed by Backscattered Electron (BSE) image. As outlined with the yellow dash lines in Fig. 6a, four distinct martensite variants in terms of crystallographic orientation with the β phase were observed in grain A. With the acquired information corresponding to the 4 α'' variants (referred as α''_1 , α''_2 , α''_3 and α''_4) and the β phase, the crystallographic orientation relationship between the original β -phase and the newly formed martensite α'' phase represented by the stereographic projections of the corresponding OR plane and OR direction was determined using the rotational coordinate transformation matrices [28–30].

To ensure the accuracy of the orientation measurement, we manually detected ten points for each variant. The mean orientation of each variant represented by Euler angles (φ_1 , Φ , φ_2) is given in Table 2. The stereographic projections of the $\{112\}_\beta$ plane and the $\langle \bar{1}10 \rangle_\beta$ direction corresponding to the β phase and the stereographic projections of the $(110)_{\alpha''}$ plane and the $[001]_{\alpha''}$ direction of the four martensite variants represented in the sample coordinate system are shown in Fig. 6b. As seen, for each martensite variant, the poles of the paired $(110)_{\alpha''}$ plane normal and the $[001]_{\alpha''}$ direction match well with the poles of the $\{112\}_\beta$ plane normal and the $\langle \bar{1}10 \rangle_\beta$ direction corresponding to the β phase. It should be mentioned that the matching directions must be contained in the matching planes. This confirms that this OR, specified as $\{112\}_\beta // (110)_{\alpha''}$ & $\langle \bar{1}10 \rangle_\beta // [001]_{\alpha''}$, is the effective one between the β phase and the α'' martensite. The results described above reveal that a four-variant net-shaped microstructure constituted of α'' martensite lamellae following the α''/β orientation

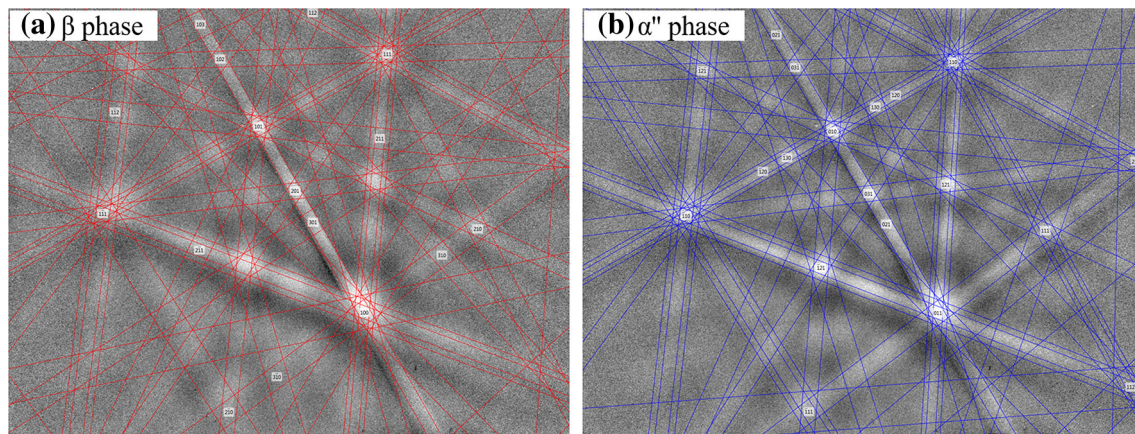


Figure 5 Kikuchi patterns corresponding to the β -phase **a** and the martensite α'' phase **b**; the calculated Kikuchi pattern for the β and α'' phases indicated by red and blue lines, respectively.

relationship, i.e., $(110)_{\alpha''} // \{112\}_{\beta}$ and $[001]_{\alpha''} // \langle \bar{1}10 \rangle_{\beta}$ is formed in the hydrogenated β -21S alloy as the hydrogen concentration increased to $H/M = 0.460$.

Hydrogen-induced phase transformation examined by TEM

Following the SEM–EBSD observations, TEM characterizations were employed to detail the hydrogen-induced microstructural modification in the hydrogenated β -21S alloys. Because of its high brittleness, traditional sample preparation techniques could not be used on the specimen of $H/M = 0.460$. All the thin foils were consequently extracted by ionic micromachining. Figure 7 shows the SEM image (obtained by In-Lens detector) of the hydrogenated specimen being prepared by ionic micromachining. To prevent the surface from an excessive erosion by the ion beam, a layer of carbon indicated with the white arrow was deposited on the selected area prior to ionic micromachining.

Figure 8a, b and c shows the selected area electron diffraction (SAED) patterns of the specimens containing H/M of 0.005, 0.100 and 0.460, respectively. For as-received β -21S alloy ($H/M = 0.005$), diffused streaks appeared in the SAED (Fig. 8a), which are associated with the athermal ω phase formed upon air quenching. Indeed, no matter how fast the cooling rate is employed, the formation of the athermal ω phase cannot be avoided in the metastable β -titanium alloys [3–7]. The observed diffused streaks in Fig. 8a indicate a very low volume fraction of athermal ω phase existed in the initial material. However, the

size of athermal ω phase is too small to resolve under the present electron beam condition.

When the hydrogen concentration increased to $H/M = 0.100$ (Fig. 8b), the intensity of the diffuse streaks associated with the athermal ω phase reduced. This observation evidenced that the addition of hydrogen promotes the stability of the β phase and inhibits the formation of the athermal ω phase upon cooling. Such phenomenon is in accordance with previous investigations in hydrogenated β -21S alloy [7, 33]. Regarding the hydrogenated sample with a high hydrogen concentration of $H/M = 0.46$, TEM thin foil was extracted from the selected area (Fig. 6a) previously localized by SEM–EBSD. Apparently, the α'' martensite lamellae still existed in the middle of the process of ionic micromachining, as indicated in Fig. 7. The associated SAED pattern (Fig. 8c) revealed that a ω -phase with two variants formed in the sample. These two variants, ω_1 and ω_2 , are highlighted with pink circles in Fig. 8c. The dark-field (DF) image corresponding to the variants ω_1 (Fig. 8d) showed that the newly formed ω phase in the form of nanoparticles (appearing as white spots) was randomly distributed in the matrix β phase. Supposing that the β phase has an orthorhombic lattice ($a = 0.3247$ nm, $b = c = \sqrt{2}a = 0.4591$ nm) [35], the volume expansion from the β to martensite α'' phase is estimated to be about 2.28%. The formation of the ω phase could then be explained by the strain relaxation upon the volume expansion from the β phase to the α'' martensite. This result is in agreement with a recent study [40] which has demonstrated that the formation of the ω phase can even be triggered by

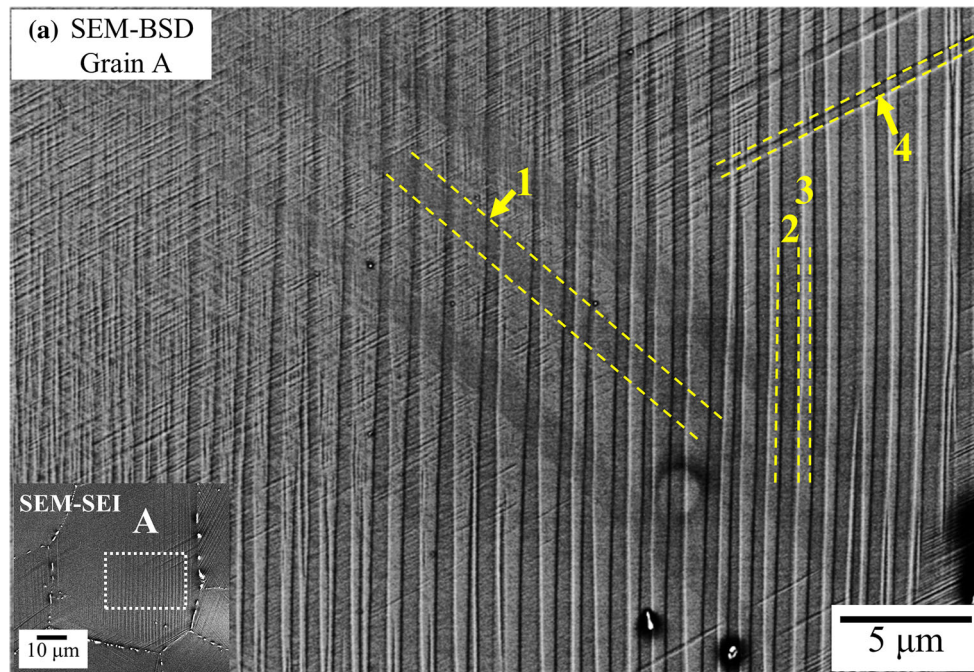
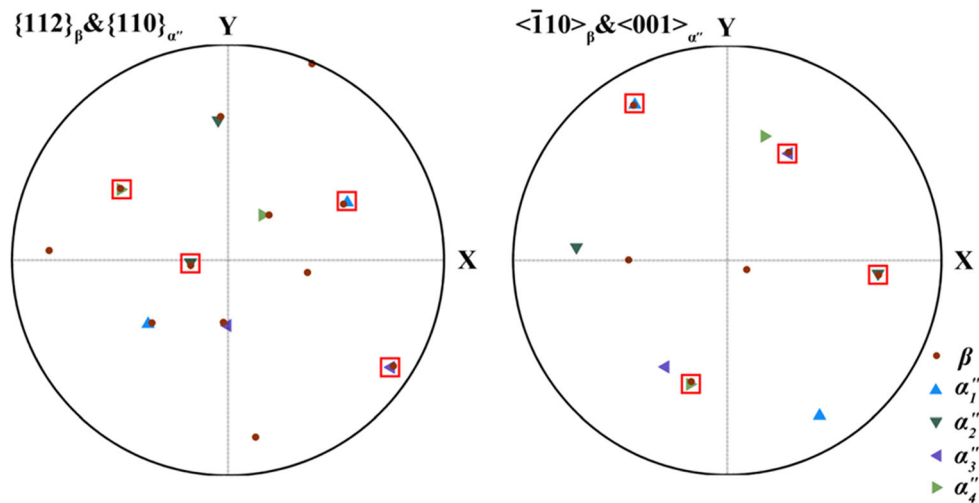
(b) OR between β -phase and α'' -martensite

Figure 6 Martensite revealed by SEM–EBSD for the sample containing $H/M = 0.460$. **a** SEM–BSE micrograph of the interest area from grain A (the inserted SEM–SEI image) and **b** the stereographic projections of the planes normal $\{112\}_\beta$ and $\{110\}_{\alpha''}$

and the directions $\langle \bar{1}10 \rangle_\beta$ and $[001]_{\alpha''}$. (the coincident projections of the β -phase and the α'' martensite are marked with red rectangles).

elastic strain or stress without plastic deformation. However, due to its low volume fraction and the limited spatial resolution of SEM, this ω phase in the form of nanosized particles cannot be detected by XRD and SEM–EBSD.

One question naturally arising from these observations is: why does the martensite α'' phase disappear after the ionic micromachining? The martensite

α'' phase is thermodynamically unstable and can spontaneously transform into stable α and/or β phases under specific conditions [8, 22, 34, 41]. In the present work, the SAED pattern taken at $H/M = 0.460$ (Fig. 8c) reveals that the martensite α'' phase has decomposed into β phase during ionic micromachining. Since the α'' martensite lamellae were still present in the middle of the process of ionic

Table 2 Crystallographic orientation information for the four variants of the α'' martensite and that of the matrix β -phase detected by EBSD

Phase	Notation	Euler angles ($\varphi_1, \Phi, \varphi_2$), ($^\circ$)
α'' martensite	α''_1	(30.76, 99.70, 173.74)
Orthorhombic	α''_2	(85.01, 70.50, 59.11)
$a = 0.3164$ nm, $b = 0.4982$ nm and $c = 0.4658$ nm	α''_3	(149.92, 59.80, 139.65)
	α''_4	(163.25, 117.76, 66.32)
β -BCC, $a = 0.3247$ nm	β	(203.58, 35.81, 10.65)

The Euler angles are presented in Bunge's notation [26, 27], which represents the mean orientation of each variants and the β phase, respectively

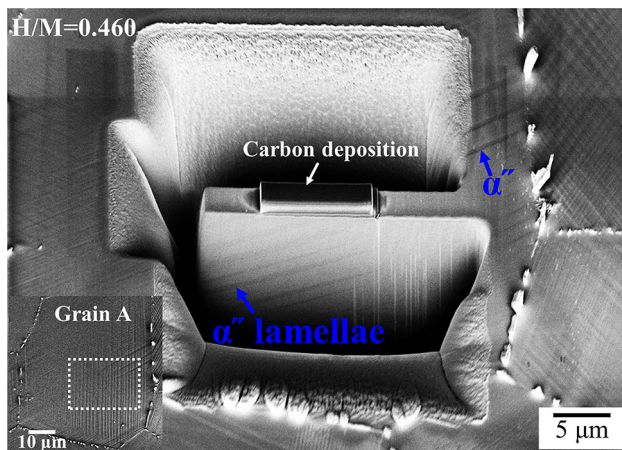


Figure 7 SEM image (In-Lens) of the hydrogenated sample being prepared by ionic micromachining with $H/M = 0.460$ (thin foil being extracted from Grain A previously localized by SEM-EBSD, as indicated by the inserted image).

micromachining (Fig. 7), the dissolution of martensite α'' phase is believed to occur at the last stage of the ionic micromachining. Additionally, stresses relaxation often occur upon ion milling [42], which can accelerate the decomposition of α'' martensitic phase into β phase.

Since martensitic transformation is a diffusionless and displacive structure transformation in solid state, it usually takes place in metastable β -titanium alloys by quenching or upon mechanical deformation [34–39]. For titanium alloys, the formation of the martensite α'' phase (orthorhombic structure) is dependent on the alloy composition and cooling rate. As far as we know, this martensite α'' phase has not been observed in the β -21S alloy upon quenching or mechanical deformation. In the present work, the martensite α'' phase is formed in the β -21S alloy upon hydrogen charging at a high hydrogen concentration. Although hydrogen can stabilize the BCC β phase to some extent Refs. [9–11, 22, 23], the formation of the

martensite α'' and ω phases at high hydrogen concentration ($H/M \geq 0.380$) indicates that the stability of β phase cannot be increased monotonically with hydrogen concentration. At lower hydrogen concentration ($H/M \leq 0.300$), the microstructure consisting of the single β -phase revealed that the interstitially dissolved hydrogen atoms expanded the BCC lattice and prevented the decomposition of the β phase upon cooling. However, at high hydrogen concentration ($H/M \geq 0.380$), the segregation of hydrogen atoms at lattice defects causes local stress concentration, which leads to anisotropic deformation of the BCC lattice. The operative mechanism behind such 'hydrogen-induced martensite transformation' is still unclear. However, a shuffling process in which atoms at each alternate $(110)_\beta$ plane move along the $[11\bar{0}]_\beta$ direction to their proper positions in the martensite structure can be a possible mechanism. Such transformation process has been proposed by Li et al. [35] through first principle calculation for Ti-xMo ($x = 4\text{--}15$ wt%) alloys. Indeed, the martensitic transformation has also been reported in unstable stainless steels during the severe cathodic hydrogen charging [43]. The authors proposed that the formation of martensite is due to the internal stresses caused by the hydrogen concentration gradient within the sample, since hydrogen was not uniformly distributed in the sample.

As an outlook, to avoid hydrogen embrittlement in β -21S alloy, the hydrogen concentration expressed as H/M should not exceed 0.3. Beyond this value, the hydrogen-induced decohesion and the formation of metastable phases (α'' and ω) occur, which inevitably reduce the strength and ductility of the material. Indeed, the effect of the hydrogen concentration on the tensile and compressive mechanical behavior has been reported in Wen's PhD thesis [44]. Though not performed under identical testing conditions, results

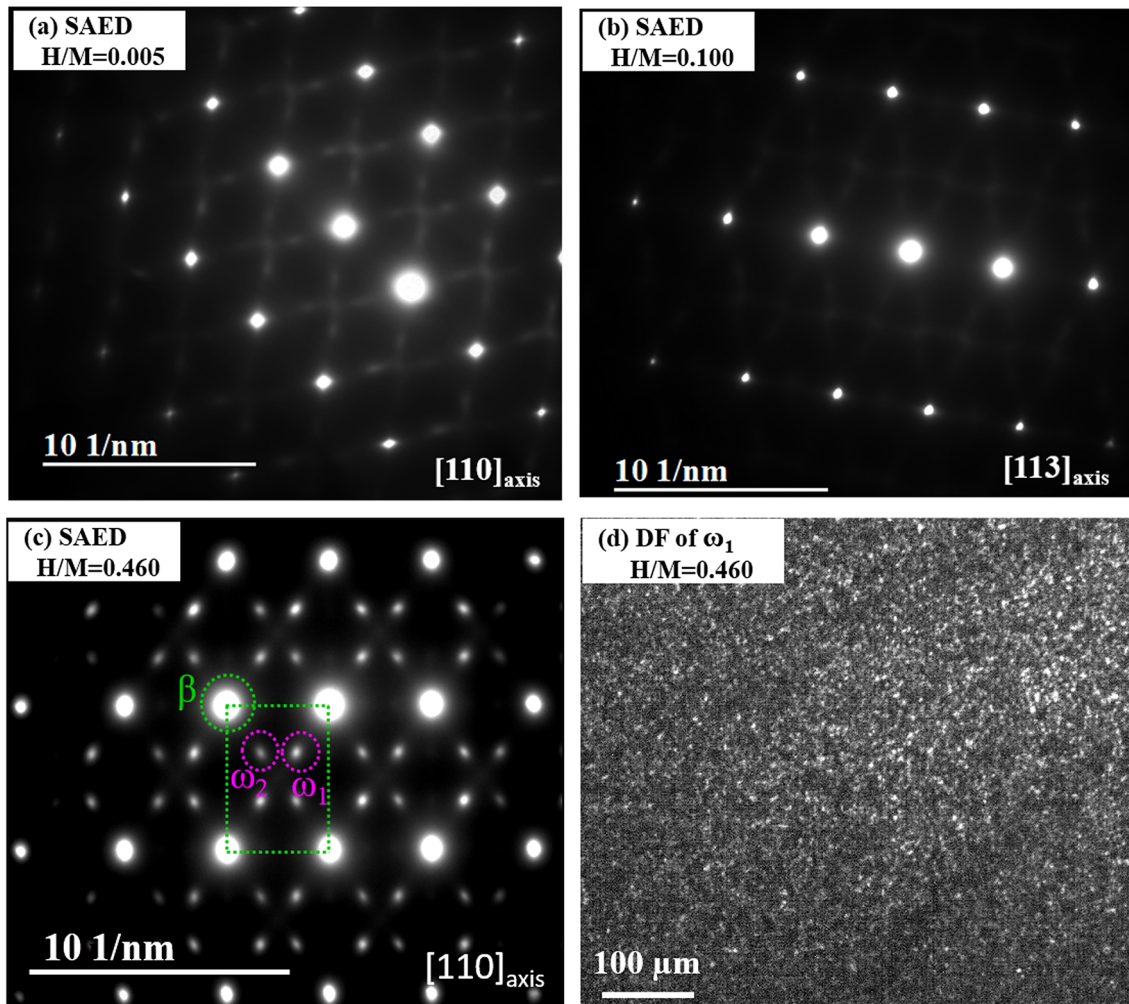


Figure 8 TEM characterization of the as-received ($H/M = 0.005$) and hydrogenated β -21S. **a** and **b** SAED patterns of the initial ($H/M = 0.005$) and hydrogenated sample with $H/M = 0.100$, respectively. **c** SAED pattern of the hydrogenated sample with

$H/M = 0.460$, the reflection of the ω_1 variant circled in pink was used to produce the DF image **d**, the white spots showing up in **(d)** being the ω precipitates with the ω_1 variant in zone axis.

in terms of strain to failure were in agreement with the work of Teter et al. [7].

Conclusions

In this work, the influence of hydrogen concentration on phase transformation and microstructure modification in the β -21S alloy was thoroughly inspected using a combined characterization by XRD, SEM-EBSD, FIB and TEM. The evolution of microstructure was found to be closely related to hydrogen concentration. For lower hydrogen concentration ($H/M \leq 0.300$), the microstructure is composed of single β -phase, revealing that the interstitially dissolved hydrogen atoms prevent decomposition of the β

phase during cooling. At higher hydrogen concentration ($H/M \geq 0.380$), an internal stress-induced phase transformation occurred; the microstructure consisted of the β phase, the α'' martensite lamellae and the nanosized ω -phase. The ω -phase produced upon the formation of the α'' martensite is ascribed to the strain relaxation caused by the volume expansion from the β phase to the α'' martensite.

Acknowledgements

Dr. Jing WEN appreciates the financial support from the French Ministry of Higher Education and Research while in LEM3. The authors are grateful to the discussion with Dr. Yudong Zhang and Dr.

Chunyang Zhang on the orientation relationships between the β -phase and the α'' martensite phase. Professor Fleury thanks the France-Korea Partenariat Hubert Curien (PHC) STAR program. This study was also supported by Ministère de l'Enseignement Supérieur, de la Recherche Scientifique et des Technologies de l'Information et de la Communication.

Data availability

All data included in this manuscript are available upon request by contact with the corresponding author.

Compliance with ethical standards

Conflict of interest The authors declare that they have no known competing financial interests or personal relationships that could have appeared to influence the work reported in this paper.

References

- [1] Bania PJ (1993). In: Eylon D, Boyer RR, Koss DA (eds) Beta titanium alloys in the 90's. TMS, Warrendale, PA, pp 3–14
- [2] Eliezer D, Böllinghaus TH (2012). 18 - Hydrogen effects in titanium alloys. In: Gangloff RP, Somerday BP (eds) Gaseous hydrogen embrittlement of materials in energy technologies, vol 2. Woodhead Publishing, pp 668–706. <https://doi.org/10.1533/9780857093899.3.668>
- [3] Correa DRN, Vicente FB, Araújo RO, Lourenço ML, Kuroda PAB, Buzalaf MAR, Grandini CR (2015) Effect of the substitutional elements on the microstructure of the Ti-15Mo-Zr and Ti-15Zr-Mo systems alloys. *J Mater Res Technol* 4:180–185
- [4] Xiao JF, Nie ZH, Tan CW, Zhou G, Chen R, Li MR, Yu XD, Zhao XC, Hui SX, Ye WJ, Lee YT (2019) Effect of reverse β -to- ω transformation on twinning and martensitic transformation in a metastable β titanium alloy. *Mater Sci Eng A* 759:680–687
- [5] Liu HH, Niinomi M, Nakai M, Cho K (2016) Athermal and deformation-induced ω -phase transformations in biomedical beta-type alloy Ti-9Cr-0.2O. *Acta Mater* 106:162–170
- [6] Chen W, Zhang JY, Cao S, Pan Y, Huang MD, Hu QM, Sun QY, Xiao L, Sun J (2016) Strong deformation anisotropies of ω -precipitates and strengthening mechanisms in Ti-10V-2Fe-3Al alloy micropillars: precipitates shearing vs precipitates disordering. *Acta Mater* 117:68–80
- [7] Teter DF, Robertson IM, Birnbaum HK (2001) The effects of hydrogen on the deformation and fracture of β -titanium. *Acta Mater* 49:4313–4323
- [8] Duerig TW, Albrecht J, Richter D, Fischer P (1982) Formation and reversion of stress induced martensite in Ti-10V-2Fe-3Al. *Acta Metall* 30:2161–2172
- [9] Froes FH, Senkov ON, Qazi JI (2004) Hydrogen as a temporary alloying element in titanium alloys: thermohydrogen processing. *Int Mater Rev* 49:227–245
- [10] Senkov ON, Froes FH (1999) Thermohydrogen processing of titanium alloys. *Int J Hydrog Energy* 24:565–576
- [11] Goltsov VA (1997) Fundamentals of hydrogen treatment of materials and its classification. *Int J Hydrog Energy* 22:119–124
- [12] Tal-gutelmacher E, Eliezer D (2004) Hydrogen-assisted degradation of titanium based alloys. *Mater Trans* 45:1594–1600
- [13] Young GA Jr, Scully JR (1993) Effects of hydrogen on the mechanical properties of a Ti-Mo-Nb-Al alloy. *Scr Met Mater* 28:507–512
- [14] Sofronis P, Robertson IM, Liang Y, Teter DF, Aravas N (2003) Hydrogen effects on material behavior and corrosion deformation interactions. In: Moody NR, Thompson AW, Ricker RE, Was GS, Jones RH (eds) TMS-AIME. Warrendale, PA, pp 537–548
- [15] Pound BG (1997) Hydrogen trapping in aged β -titanium alloys. *Acta Mater* 45:2059–2068
- [16] Robertson IM, Sofronis P, Nagao A, Martin ML, Wang S, Gross DW, Nygren KE (2015) Hydrogen embrittlement understood. *Metall Mater Trans A* 46A:2323–2341
- [17] Eliezer D, Tal-gutelmacher E, Cross CE, Boellinghaus T (2006) Hydrogen trapping in β -21S titanium alloy. *Mater Sci Eng A* 421:200–207
- [18] Troiano AR (2016) The role of hydrogen and other interstitials in the mechanical behavior of metals. *Metallogr Microstruct Anal* 5:557–569
- [19] Hanneken JW (1999) Hydrogen in metals and other materials: a comprehensive reference to books, bibliographies, workshops and conferences. *Int J Hydrog Energy* 24:1005–1026
- [20] Shivanyuk VN, Shanina BD, Tarasenko AV, Gavriljuk VG, Foc J (2001) Effect of hydrogen on atomic bonds in austenitic stainless steel. *Scr Mater* 44:2765–2773
- [21] Nagao A, Dadfarnia M, Somerday BP, Sofronis P, Ritchie RO (2018) Hydrogen-enhanced-plasticity mediated decohesion for hydrogen-induced intergranular and “quasi-cleavage” fracture of lath martensitic steels. *J Mech Phys Solids* 112:403–430

- [22] Qazi JI, Senkov ON, Rahim J, Genc A, Froes FH (2001) Phase transformations in Ti-6Al-4V-xH Alloys. *Metall Mater Trans A* 32:2453–2461
- [23] Kirchheim R (2007) Reducing grain boundary dislocation line and vacancy formation energies by solute segregation. I. theoretical background. *Acta Mater* 55:5129–5138
- [24] Cao F, Kumar P, Koopman M, Lin C, Fang Z, Ravi Chandran KS (2015) Understanding competing fatigue mechanisms in powder metallurgy Ti-6Al-4V alloy: role of crack initiation and duality of fatigue response. *Mater Sci Eng A* 630:139–145
- [25] Cao F, Ravi Chandran KS, Kumar P, Sun P, Fang Z, Koopman M (2016) New powder metallurgical approach to achieve high fatigue strength in Ti-6Al-4V alloy. *Metall Mater Trans A* 47(5):2335–2345
- [26] Bunge HJ, Esling C, Muller J (1981) The influence of crystal and sample symmetries on the orientation distribution function of the crystallites in polycrystalline materials. *Acta Cryst A* 37:889–899
- [27] Bunge HJ, Esling C, Muller J (1980) The role of the inversion centre in texture analysis. *J Appl Cryst* 13:544–554
- [28] Miyamoto G, Takayama N, Furuhashi T (2009) Accurate measurement of the orientation relationship of lath martensite and bainite by electron backscatter diffraction analysis. *Scr Mater* 60:1113–1116
- [29] Nolze G, Geist V (2004) A new method for the investigation of orientation relationships in meteoritic plessite. *Cryst Res Tech* 39:343–352
- [30] Wen J, Allain N, Fleury E (2020) Determination of orientation relationships between FCC-hydride and HCP-titanium and their correlation with hydrides distribution. *J Alloys Compd* 817(9):153297
- [31] Tal-gutelmacher E, Eliezer D, Boellinghaus T (2007) Investigation of hydrogen-deformation interactions in β -21S titanium alloy using thermal desorption spectroscopy. *J Alloys Compd* 440:204–209
- [32] Materials Analysis Using Diffraction (MAUD): <http://maud.radiographema.eu/>.
- [33] Sankaran SN, Herrmann RK, Wiedemann KE, Shenoy RN (1994) Microstructure/Property relationships in titanium alloys. TMS, Warrendale, PA, p 215
- [34] Mantani Y, Takemoto Y, Hida M, Sakakibara A, Tajima M (2004) Phase transformation of α'' martensite structure by aging in Ti-8 mass% Mo alloy. *Mater Trans* 45:1629–1634
- [35] Li M, Min X, Yao K, Ye F (2019) Novel insight into the formation of α'' -martensite and ω -phase with cluster structure in metastable Ti-Mo alloys. *Acta Mater* 164:322–333
- [36] Yao TT, Du K, Wang HL, Huang ZY, Li CH, Li LL, Hao YL, Yang R, Ye HQ (2017) In situ scanning and transmission electron microscopy investigation on plastic deformation in a metastable β titanium alloy. *Acta Mater* 133:21–29
- [37] Paradkar AG, Kamat SV, Gogia AK, Kashyap BP (2007) Various stages in stress-strain curve of Ti-Al-Nb alloys undergoing SIMT. *Mater Sci Eng A* 456:292–299
- [38] Paradkar AG, Kamat SV, Gogia AK, Kashyap BP (2008) Effect of Al and Nb on the trigger stress for stress-induced martensitic transformation during tensile loading in Ti-Al-Nb alloys. *Mater Sci Eng A* 487:14–19
- [39] Kim HY, Ikehara Y, Kim JI, Hosoda H, Miyazaki S (2006) Martensitic transformation, shape memory effect and superelasticity of Ti-Nb binary alloys. *Acta Mater* 54:2419–2429
- [40] Liu H, Niinomi M, Nakai M, Cho K, Fujii H (2017) Deformation-induced ω -phase transformation in a β -type titanium alloy during tensile deformation. *Scr Mater* 130:27–31
- [41] Barriobero-Vila P, Oliveira VB, Schwarz S, Buslaps T, Requena G (2017) Tracking the α'' martensite decomposition during continuous heating of a Ti-6Al-6V-2Sn alloy. *Acta Mater* 135:132–143
- [42] Spurling RA, Rhodes CG, Williams JC (1974) The microstructure of Ti alloys as influenced by Thin-Foil artifacts. *Metall Trans* 5:2597–2600
- [43] Rozenak P, Zevin L, Eliezer D (1984) Hydrogen effects on phase transformations in austenitic stainless steels. *J Mater Sci* 19:567–573
- [44] J. Wen (2017) Effect of hydrogen on the microstructure and cold rolling behavior of commercially pure titanium and β -Metastable titanium Alloy. PhD Dissertation, Université de Lorraine. English. NNT: 2017LORR0167.

Publisher's Note Springer Nature remains neutral with regard to jurisdictional claims in published maps and institutional affiliations.